Reference :

F. Radjaï, H. Troadec, and S. Roux (2004)
in "Granular Materials: Fundamentals and Applications"
edited by S.J. Antony, W. Hoyle and Y. Ding
The Royal Society of Chemistry, Cambridge,
Pages 157-184

KEY FEATURES OF GRANULAR PLASTICITY

F. Radjaï[1], H. Troadec[1] and S. Roux[2]

[1]LMGC, CNRS-Université Montpellier II,
Place Eugène Bataillon,
34095 Montpellier cedex, France.

[2]LSVI, CNRS-Saint Gobain,
39 Quai Lucien Lefranc,
93303 Aubervilliers Cedex, France

Email: radjai@lmgc.univ-montp2.fr

1 THE MYSTERY OF SAND

Sand and other cohesionless or weakly cohesive granular materials share marked *plastic* properties which reflect their common *granular structure*. Intuitively, we understand the flow and irrecoverable deformations of sand as an evident consequence of the relative displacements of the grains (seen as solid particles interacting via contact and friction) caused by an external mechanical action. The mystery is that, this desperately simple (and correct) picture of granular plasticity does not let itself be captured into an equally simple model thoroughly based on the properties of the grains and their organization in space. Recent interdisciplinary research on the matter has even transformed the status of sand as a rather old poetic symbol of simplicity into a paradigm of *complexity*![1] This metamorphose is motivated by the observation that dry granular materials behave very differently both from ordinary molecular fluids when they flow and from ordinary solids when they remain at rest.[2] Obviously, an extraordinarily rich behaviour emerges when simple grains are piled to form a granular structure.

The experimental observation of force inhomogeneity[3] and structural anisotropy[4] in model particle assemblies about four decades ago suggested that a detailed description of granular *microstructure* should provide a key for understanding the quasistatic rheology of granular

materials. For two decades, such a description has been offered by *distinct element* numerical simulations.[5,6] The elements are idealized grains (discs, polygons … in two dimensions, spheres, polyhedra … in three dimensions). The equations of motion of each grain are integrated by taking into account contact interactions and body or boundary forces and displacements. It happens that, even with most basic ingredients, a rich behaviour is observed as in experiments. The simulations provide detailed information about grain motions and contact forces. Fascinating phenomena, such as the *bimodal* transmission of stresses[7] and *collective* particle motions at intermediate scales between the grain size and the system size,[8,9] can be observed. Yet, such often intriguing phenomena have in many ways helped more to reinforce the mystery of sand than to unravel it.

The difficulty here is common to all heterogeneous materials: what is the simplest level of microstructural information, and to what extent does it control the effective properties of the material? How do the effective properties depend on higher-order microstructural information? The phase volume fractions often provide trivial first-order information. In the case of a dry granular material, we distinguish the solid phase from the pore phase. The *solid fraction* ρ (volume fraction occupied by the grains) is known to influence strongly the shear strength and stress-strain behaviour.[10,11] However, the mean coordination number z (the average number of contact neighbours of a grain) can be used, as well, as a descriptor of the average *compactness* of the structure. But, the choice between ρ and z is not a mere matter of taste since the idea is to account properly for *grain scale* mechanisms. The point is that the grains interact via *contact* and this property is an essential ingredient of granular materials. The equilibrium and motion of a grain are thus more related to its *contact neighbours* than to the average free volume accessible to the grain. This implies that the coordination number is more suitable than the solid fraction as state variable.

Recognizing the coordination number z as the *lowest-order* relevant microstructural information, represents already a step beyond the phenomenological approach. This is also a rewarding choice as it naturally points to higher order microstructural information. In fact, the coordination number, as an average over all grains in a control volume, does not make much sense to the grains have which always an *integer* number of contact neighbours. Hence, a more detailed description of the microstructure requires the *connectivity* function $p_c(c)$, defined as the fraction of grains with exactly c contact neighbours.

In order to describe the grain equilibrium states, which underlie the yield properties of a granular medium, further information is required about the angular positions of the contact neighbours. For this purpose, one may rely on the *fabric tensors* of increasing order ($\vec{n} \otimes \vec{n}$, $\vec{n} \otimes \vec{n} \otimes \vec{n} \otimes \vec{n}$, etc) constructed from contact normals $\vec{n}$, or resort to the 1-contact probability density function $p(\vec{n})$ defined as the probability that a contact normal is oriented along $\vec{n}$.[12] An exact description of the environment of a grain requires, however, *multi-contact* probability density functions $g_c(\vec{n}_1, \vec{n}_2, \ldots, \vec{n}_c)$ corresponding to the probability that the contact neighbours (for a grain with c contact neighbours) occupy the angular positions $(\vec{n}_1, \vec{n}_2, \ldots, \vec{n}_c)$ around the grain.[13,14] Both p_c and g_c are controlled by steric exclusions of the grains and they depend on the *composition* (grain shapes and size distribution). More importantly, they evolve with plastic strain.

We see that the *steric constraints* (mutual exclusions together with excluded-volume effects that impose an upper bound on the number of contact neighbours) result in a dependence of the yield properties of a granular medium on nontrivial features of the microstructure (beyond the solid fraction). This is also true for the flow properties (dilatancy)

which require the compatibility of the global imposed strain with local steric constraints. In the same way, the hardening properties reflect the evolution of the microstructure which involves both discontinuous changes, due to creation and loss of contacts between the grains, and distortions as a result of the rotations of persisting contact normals.

The apparent mystery of granular materials reflects not only the complexity of their microstructure but also the fact that the effective plastic properties involve nontrivial details of this microstructure and its evolution. The ambition of this contribution is not to present a model of granular plasticity based on the microstructure though this is obviously the long term scope of this work. Instead, we discuss a number of basic behaviours in the light of simple microstructural considerations by indicating at each step the route to a more fundamental approach. In particular, we emphasize the role of steric constraints, compactness and structural anisotropy, retained as the most salient microstructural information, with respect to shear strength, stress-strain and volume-change properties in model granular media composed of rigid (two-dimensional) disks interacting via contact and friction.

2 GRANULAR FRICTION

The granular microstructure can be seen as the disordered grain configuration that spans the space from the contact scale to the system boundaries. The query is how this microstructure controls the scale-up of the contact rheology (local behaviour) to the macroscopic scale (global behaviour). Within the hard-particle approximation, assumed here, the contact rheology is approximated by two ``contact laws'': the Signorini condition (mutual exclusion of the grains) and the Coulomb friction law. The Signorini condition simply relates the distance δ between two particles and the corresponding normal reaction force N: For $\delta \neq 0$ (no contact), the normal force is zero, $N = 0$, whereas for $\delta = 0$ (contact), N can take arbitrarily large positive (compressive) values. This relation is shown as a graph in Figure1(a). This is a *nonsmooth* relation in the sense that the set of admissible pairs (δ, N) can not be reduced to a (mono-valued) function.[15-17] On the other hand, the Coulomb friction law relates the tangential force T and the sliding velocity v_s at contacts between grains. Again, the set of admissible pairs (v_s, T), shown as a graph in Figure1(b), can not be reduced to a function: at $v_s = 0$, the friction force T can take any value in the range $[-T_s, T_s]$, with $T_s = \mu N$, where μ is the coefficient of friction. The Coulomb friction law and the Signorini condition have the remarkable property that they involve *no force scale*. The range of admissible contact forces $\vec{f} = (N, T)$ is inside a cone $T_s = \mu N$ with $N > 0$.

As a result of the absence of intergrain forces of cohesion ($N > 0$), the stress state is, for the most part, controlled by the boundary stresses and bulk forces. Classically, the Cauchy stress tensor $\overline{\overline{\sigma}}$ in a static granular medium is an average quantity involving contact forces $\vec{f} = (N, T)$ and intercentre vectors $\vec{l}$ joining the centres of contact neighbours:[18-20]

$$\overline{\overline{\sigma}} = n_c \left\langle \vec{f} \otimes \vec{l} \right\rangle \qquad (1)$$

The symbol $\otimes$ stands for dyadic product and n_c is the number density of contacts. The averaging $\langle ... \rangle$ runs over the whole contact set in a control volume. Since $\overline{\overline{\sigma}}$ is linear in $\vec{f}$, and the forces belong to a cone, the domain of admissible stresses is also necessarily inside a cone $\tau_s = M\nu$ with $\nu > 0$ (compressive) in the stress space, where $\tau_s \equiv \vec{n}\overline{\overline{\sigma}}\vec{t}$ and $\nu \equiv \vec{n}\overline{\overline{\sigma}}\vec{n}$ are respectively the shear and normal stresses on the yield plane (line, in two dimensions) characterized by its normal and tangential unit vectors $\vec{n}$ and $\vec{t}$, and M is a *global* (or effective) coefficient of friction.

The above argument recovers the Coulomb yield criterion, with $\varphi = \tan^{-1}(M)$ corresponding to the *internal angle of friction*. Equivalently, the stress ratio q/p, where p and q are the mean and deviator stresses respectively, is given by $q/p = \sin\varphi$. The important point here is that, this argument does not refer to the microstructure, so that M is defined *whatever* the mechanical state of the medium. The usual Coulomb yield criterion corresponds only to the steady state (the "critical state" of soil mechanics[21]) which is a particular state of the material (reached upon sufficient monotonic shearing and in which no volume change occurs). The Coulomb model is thus a *rigid-plastic* behaviour without state variables (no evolution of the microstructure). This model can be considered as a simple scale-up of contact friction with the yield plane (determined *a posteriori*) playing the same role as the contact plane between two grains (fixed *a priori*). Since the material is assumed to possess a unique state, corresponding to a unique microstructure that does not evolve, *the* internal angle of friction φ in the Coulomb model is an intrinsic property of the material.

However, since the internal angle of friction φ is defined whatever the microstructure, the Coulomb model can readily be generalized to arbitrary states through the dependence of φ on the microstructure.[13,22] In other words, assuming that p_c and g_c contain the relevant microstructural information, the yield properties of a granular material are characterized by the function $\varphi = \varphi(p_c, g_c)$. Upon shearing, the distributions p_c and g_c evolve incrementally with plastic strain $\dot{\varepsilon}_s$: $\dot{p}_c = \dot{p}_c(\dot{\varepsilon}_s, p_c, g_c)$ and $\dot{g}_c = \dot{g}_c(\dot{\varepsilon}_s, p_c, g_c)$. The steady state corresponds to $\dot{p}_c(\tilde{p}_c, \tilde{g}_c) = \dot{g}_c(\tilde{p}_c, \tilde{g}_c) = 0$, where $\tilde{p}_c$ and $\tilde{g}_c$ are steady-state distribution functions. Hence, in this framework the internal angle of friction is *state dependent*, only the steady-state value $\tilde{\varphi}(\tilde{p}_c, \tilde{g}_c)$ being a material property. In the following, we will discuss the potential predictions of this generalization of the Coulomb model to include state variables pertaining to the microstructure.

3 THE FABRIC

The distributions g_c and p_c contain rich information about local structures characterized by the positions of contact neighbours in the angular interval $[0,2\pi[$ around a typical grain with c contact neighbours. The drawback with an approach based on too detailed microstructural information is that it requires simplifications at the level of the composition and resort to numerical procedures in order to obtain quantitative results. In fact, discrete element simulations can be seen as an extreme approach totally based on *all* details of the microstructure (positions and velocities of all grains). This approach provides quantitative results and, due to the fast increase of the available computer power and memory, it can be

used as a precious investigation tool in the domain of granular materials. But because of the profusion of information, it does not readily help to get insight into the behaviour. In a microscopic approach, a useful strategy is to begin with the lowest-order microstructural information and to enrich the description by including higher order information in a progressive manner.[13]

Key information contained in g_c is the *angular exclusions*: the angular positions of contact neighbours around a grain are such that, due to their mutual hindrances, there is a finite difference between them always larger than an *exclusion angle* $\delta\theta_{\min}$ (see Figure 2), so that[13,14]

$$g_c = 0 \quad \Leftrightarrow \quad \vec{n}^{\alpha} \cdot \vec{n}^{\beta} < \cos(\delta\theta_{\min}) \tag{2}$$

The exclusion angle is about $\pi/3$ for grains of nearly the same size. The angular exclusions, as a local property of the granular structure, obviously play a key role in yield, flow and hardening properties of a granular medium by virtue of the constraints they impose on grain motions and accessible equilibrium states.

The coordination number $z = \sum_c c\, p_c$ describes the average connectivity of granular structure. An equivalent parameter is the valence number v, defined as the average number of edges per void cell (a loop of contiguous grains surrounding a pore).[8] The Euler formula for the grain network allows us to relate the valence number to the coordination number: $v = 2z/(z-2)$. The coordination number is limited by an upper bound $z_{\max}$ as a result of angular exclusions. $z_{\max}$ is equal to 6 for grains of tight polydispersity (weak size dispersion) in two dimensions in the presence of long-range (crystalline) order and equal to 4 in the presence of disorder.[23] There is also a lower bound $z_{\min}$ imposed by the requirement of grain equilibrium. Numerical simulations show that, although a grain can in principle be equilibrated under the action of *two* frictional contact forces, the coordination number never decreases below 3.

Other basic information included in the function g_c is the 1-contact distribution function $p_\theta(\theta)$ of contact directions θ which is obtained by integrating $\sum_c p_c\, g_c$ over all angles except one. Notice that, due to angular exclusions, the multi-contact distribution g_c is not a product of 1-contact distribution functions: $g_c(\theta_1,\ldots,\theta_c) \neq p_\theta(\theta_1)\ldots p_\theta(\theta_c)$. The distribution p_θ is easily accessible from (two-dimensional) experiments and simulations, and it has been extensively investigated in the past.[4,7,19,20,24] A fundamental observation is that p_θ is not uniform: there are preferred contact directions. In other words, the granular structure is generically *anisotropic*. This bias in contact directions is induced by the relative motions of grains: contacts are gained along the directions of compression and lost along the directions of extension. This means that, starting from an isotropic packing and applying a monotonic homogeneous shearing, the function p_θ is expected to tend to a simple form reflecting the elongational deformation in different directions, namely $p_\theta = (1/2\pi)\big(1 + a\cos 2(\theta - \theta_c)\big)$, where a represents the *anisotropy* of the packing, and θ_c is the average contact direction. Indeed, this simple form, with two parameters a and θ_c characterizing the anisotropy and its direction, provides a reasonable fit for a number of numerical and experimental data;[19,24] see

Figure 3. The values of a and θ_c can be more conveniently extracted from the fabric tensor $\overline{\overline{F}} = \langle \vec{n} \otimes \vec{n} \rangle$.[12] It is easy to show that $a = 2(F_1 - F_2)$, where $F_{1,2}$ are the eigenvalues, and θ_c is the major principal direction of the fabric tensor.

Retaining a, θ_c and z as the only relevant state variables, the functions g_c and p_c can be constructed by requiring that their informational content is strictly equivalent to the angular exclusions, on one hand, and to the knowledge of a, θ_c and z, on the other hand.[13,14] In other words, the neglected information is simply replaced by *disorder*. In practice, this amounts to maximizing the statistical entropy associated with g_c and p_c constrained by the available information. The estimated distributions g_c by means of this method have been shown to compare well with numerical simulations in the steady state for $c = 4$ and $c = 5$ in two dimensions.[14]

4 SHEAR STRENGTH

The anisotropy of the structure has a fundamental implication: the failure criterion φ can not be isotropic as in the basic Coulomb model. This means that the shear strength for an anisotropic microstructure varies with the direction of loading. In practice, this effect is more visible on the stress-strain behaviour in different directions and it has been observed in experiments.[10] This effect is particularly important when the direction of shear is reversed (unloading) in which case a long transient shear occurs before the critical state in a new direction is reached.[24] Let us recall that the basic Coulomb model (with an isotropic failure criterion) simply predicts that the system remains in the critical state for all shear directions.

The dependence of the internal angle of friction on structural anisotropy a is a direct consequence of the fact that the distribution p_θ enters the micromechanical expression of the stress tensor (Equation 1). Setting $\vec{f} = N\vec{n} + T\vec{t}$, $\vec{l} = l\vec{n}$ and $\vec{n} = (\cos\theta, \sin\theta)$ for a two-dimensional packing of disks and neglecting the correlations between l and N (nearly absent in two dimensions), the expression of the stress tensor yields the following equations for the mean stress p and the deviatoric stress q:

$$p = \frac{n_c l_m}{2} \langle N \rangle \tag{3}$$

$$q = \frac{n_c l_m}{2} \left(\langle N \cos 2(\theta - \theta_\sigma) \rangle + \langle T \sin 2(\theta - \theta_\sigma) \rangle \right) \tag{4}$$

where l_m is the mean intercentre distance. Notice that the two terms of the expression of q in Equation 4 correspond to the *correlation* between the force amplitude (N or T) and the contact direction (θ).

The measure for the averaging operation $\langle \cdots \rangle$ in its integral form is $p_e(\theta, N, T)\, d\theta\, dN\, dT$ (the average of a quantity A is given by $\langle A \rangle = \int A\, p_e\, d\theta\, dN\, dT$). The probability distribution function $p_e(\theta, N, T)$ is the probability for a contact to have its direction along θ and to carry

normal and tangential forces N and T, respectively. By definition, $p_\theta(\theta) = \int p_e \, dN \, dT$. The distribution p_e allows also to define the average forces $N_m(\theta)$ and $T_m(\theta)$ by

$$N_m(\theta)\, p_\theta(\theta) \equiv \int N \, p_e \, dN \, dT \tag{5}$$

$$T_m(\theta)\, p_\theta(\theta) \equiv \int T \, p_e \, dN \, dT \tag{6}$$

In the absence of correlations, Equation 4 implies $q = \frac{n_c \, l_m}{2}\left(\langle N\rangle\langle\cos 2(\theta-\theta_\sigma)\rangle + \langle T\rangle\langle\sin 2(\theta-\theta_\sigma)\rangle\right)$. But, due to equilibrium, we have $\langle T\rangle = 0$, so that $q/p = \langle\cos 2(\theta-\theta_\sigma\rangle$. For an isotropic structure ($p_\theta(\theta) = 1/2\pi$), this implies $q/p = 0$. For an anisotropic structure, the largest value of the stress ratio q/p is obtained if the distribution $p_\theta(\theta)$ of contact directions varies as $\cos 2(\theta-\theta_c)$ with $\theta_c = \theta_\sigma$. This implies *coaxiality* between the fabric tensor $\overline{\overline{F}}$ and the stress tensor. Then, the Fourier expansion

$$p_\theta(\theta) = \frac{1}{2\pi}\left[1 + a\cos 2(\theta-\theta_c) + \cdots\right] \tag{7}$$

where a is the amplitude of anisotropy, yields $q/p = \int_0^{2\pi} p_\theta(\theta)\cos 2(\theta-\theta_c)\, d\theta = a/2$. Note that for the largest anisotropy $a = 1$ (which can never happen due to structural disorder), the largest stress ratio is $q/p = 1/2$, corresponding to $\varphi = 30°$.

The simulations show, however, a strong correlation between the forces and the contact directions.[19] According to Equation 4, the stress ratio is maximized with respect to θ if N varies as $\cos 2(\theta-\theta_\sigma)$, T varies as $\sin 2(\theta-\theta_\sigma)$ and $p_\theta(\theta)$ varies as $\cos 2(\theta-\theta_\sigma)$. Of course, it is highly improbable that this should happen individually for each contact, but the average forces $N_m(\theta)$ and $T_m(\theta)$ as a function of contact direction do show this behaviour in a monotonic deformation.[19] More generally, starting with a given fabric, the stresses can be applied in *arbitrary* directions, and fabric changes are not immediate. From Equation 4 and using the Fourier expansions

$$N_m(\theta) = \langle N\rangle\left[1 + a_n\cos 2(\theta-\theta_n) + \cdots\right] \tag{8}$$

$$T_m(\theta) = \langle N\rangle\left[a_t \sin 2(\theta-\theta_t) + \cdots\right] \tag{9}$$

where θ_n and θ_t are the preferred directions of N_m and T_m, we get

$$\frac{q}{p} = \frac{a_n}{2}\cos 2(\theta_\sigma-\theta_n) + \frac{a_t}{2}\cos 2(\theta_\sigma-\theta_t) + \frac{a}{2}\cos 2(\theta_\sigma-\theta_c) \tag{10}$$

where cross products among the anisotropies a, a_n and a_t have been neglected. This is an interesting relation as it shows that the shear strength depends on the direction of loading (as expected from the anisotropy of the structure). It is important to remark that the presence of an anisotropic fabric that is not coaxial with the stress tensor breaks the chiral (left-right) symmetry of the problem with respect to the principal stress directions. This means that, in order to interpret correctly the phase differences in Equation 10, one should ensure that the amplitudes a, a_n and a_t, as well as q, all have the same sign, e.g. positive.

Equation 10 separates two microstructural origins of the shear strength in a granular packing: 1) structural anisotropy, represented by the parameter a; 2) force anisotropy captured into the parameters a_n and a_t. The parameters a_n and a_t can be considered also as structural properties that, in the last analysis, are linked with the anisotropy a. This link is complex, involving the microstructure beyond the first neighbours due to force correlations. Since the anisotropy and phase differences are internal (hardening) parameters from a micromechanical point of view, the expression of the stress ratio in Equation 10 can be interpreted as that of the *yield* stress ratio $\sin\varphi$ for a given set of internal parameters. Then, θ_σ should be replaced by space direction θ. On the other hand, we have to set $\varphi = 0$ for the directions that lead to a negative value of the deviator stress. Starting with an arbitrary initial state, *monotonic* shearing tends to bring the structure to a force-fabric coaxial state $\theta_c = \theta_n = \theta_t$. In this case, we have $\varphi = 0$ for $\theta_c + \pi/4 < \theta < \theta_c + 3\pi/4$ since q in Equation 10 is negative for these directions. The expression of the internal angle of friction becomes

$$\sin\varphi = \begin{cases} \frac{1}{2}(a_n + a_t + a)\cos 2(\theta - \theta_c) & \text{if } \theta < \theta_c + \pi/4 \text{ or } \theta_c + 3\pi/4 < \theta \\ 0 & \text{if } \theta_c + \pi/4 \le \theta \le \theta_c + 3\pi/4 \end{cases} \qquad (11)$$

The largest value of the shear strength is then $q/p = (a + a_n + a_t)/2$ occurring in the direction $\theta = \theta_c$.[19] When the stress principal axes rotate, phase differences may still persist even in monotonic shearing. Then, according to Equation 10, the shear strength is lower than $(a + a_n + a_t)/2$ due to those phase differences.

5 STRESS-STRAIN BEHAVIOUR

The compactness, in terms of the solid fraction ρ or the coordination number z, does not enter the expression of the stress ratio in Equation 10. At first sight, this might appear in contradiction with the observation that the stress-strain behaviour is crucially dependent on the initial compactness of a granular sample. We know also from experiments that when an initially isotropic assembly is subjected to shearing, the stress ratio always increases with shear strain whatever the initial density, whereas the density either increases, if the initial state is loose, or decreases, if the initial state is dense.[10] Here, we would like to show that these behaviours are reconciled if the shear strength depends only *implicitly* on the compactness through the anisotropy, the *accessible* anisotropies to the microstructure being constrained by the compactness.

There are two ways to evaluate these constraints: from the grain-scale environments or from a global point of view. Let us first consider one grain with its c contact neighbours, all having nearly the same size so that the exclusion angle is $\pi/3$ (see Figure 2). The components of the local fabric tensor associated with the grain are $F_{ij} = (1/c)\sum_{\alpha=1}^{c} n_i^\alpha n_j^\alpha$, where $\vec{n}^\alpha$ is the normal unit vector of the contact α. Maximizing the anisotropy $a = 2(F_1 - F_2)$ in the presence of steric constraints Equation 2 yields:[14]

$$a_{\max}(c) = \frac{2\pi}{3\sqrt{3}}\left(\frac{c_{\max}}{c} - 1\right) \tag{12}$$

where $c_{\max}$ is the largest possible number of contact neighbours. Equation 12 shows that $a_{\max}$ increases nonlinearly from 0 for $c = 6$ to ≈ 2.4 for $c = 2$. Of course, the largest local anisotropy, by definition, is 2. For $c = 4$, we get $a_{\max} \approx 0.6$. The corresponding configuration is shown in Figure 4. Due to disorder, the largest anisotropies observed in two dimensions for slightly polydisperse systems are much lower (less than 0.2).

Alternatively, we may arrive at an expression for $a_{\max}$ by considering that all microstructural states of a granular assembly are enclosed between two *isotropic limit state*: (1) the *densest* isotropic state, characterized by $z_{\max}$ or $\rho_{\max}$, and (2) the *loosest* isotropic state, characterized by $z_{\min}$ or $\rho_{\min}$. These limit states are more difficult to reach than the steady state. In particular, it is generally difficult to bring a granular system towards a dense isotropic state by means of isotropic compaction. The reason is that the rearrangements occur mainly in the presence of shearing, and the latter induces structural anisotropy. Let us also mention here the concept of *random close packing* which refers to the densest disordered packing. This concept is not well-defined since the "randomness" to which its definition refers has not been specified in terms of the microstructure.[25] For example, relying only on the compactness and anisotropy as the relevant microstructural information, there is a continuous set of randomly close-packed systems for the anisotropy varying from zero to its largest value. The densest isotropic state does not need to be disordered. In two dimensions and for a monodisperse system, it corresponds to a triangular network with $z_{\max} = 6$ and $\rho_{\max} = 0.91$. In the absence of long-range correlations in contact directions, both z and ρ are always below these values. If the requirement of randomness in contact directions (no short-range correlations) is added, then $z_{\max} \approx 4$.[23] In practice, partial crystallisation may occur spontaneously in the presence of gravity or flat walls, allowing z to exceed 4.

In general, $z_{\max}$ and $\rho_{\max}$ are controlled by steric constraints, whereas $z_{\min}$ or $\rho_{\min}$ are clearly related to the condition of grain equilibrium. The latter (in the absence of rolling strength between grains) implies that the fraction of grains with $c = 2$ can not be large. As a result, a loose isotropic packing should be constructed with $c = 3$. To reach the loosest structure, the pore volume fraction should be maximized. At the grain scale, it amounts to maximizing the area of a void cell. The valence number in a packing with $z = 3$, is $v = 6$, and simple geometry shows that *regular* hexagons (assuming that the distances between grain centres are all equal) have the largest area for a fixed circumference. As a result, the loosest local structure with $c = 3$ has also the property to be isotropic (the regularity of a polygon implies isotropy of the corresponding fabric). Hence, the loosest isotropic state may be

identified with a hexagonal (honeycomb) packing with $z_{\min} \approx 3$ and $\rho_{\min} = \pi/3\sqrt{3} \approx 0.6$. Obviously, still looser structures with lower coordination numbers may be constructed and similar arguments may be used, but such structures are unstable due to the presence of grains with two contacts (contact chains). In fact, none of the two isotropic limits with $z = 3$ and $z = 6$ can be reached in practice. But, as *reference* states, they provide an intuitive representation of the limit isotropic states and their properties.

In order to characterize the geometrical states by a single function, let us introduce the function $E(\theta) = z\, p_\theta(\theta)$. This is the distribution of contact directions normalized by the coordination number, so that $\int_0^{2\pi} E(\theta)\, d\theta = z$. The two limit isotropic states are then represented by $E_{\max}(\theta) = z_{\max}/2\pi$ and $E_{\min}(\theta) = z_{\min}/2\pi$. Equivalently, we introduce the fabric tensor $\overline{\overline{G}} \cong z\,\overline{\overline{F}}$ with eigenvalues $G_1 = z F_1$ and $G_2 = z F_2$. The limit isotropic states correspond to $G_1 = G_2 = G_{\min} = z_{\min}/2$ and $G_1 = G_2 = G_{\max} = z_{\max}/2$. Let z ($\in [z_{\min}, z_{\max}]$) be the current coordination number. Starting with an isotropic distribution $E(\theta) = z/2\pi$, we may construct an anisotropic distribution with a fixed value of z by adding contacts in one direction, θ_c, and removing as many contacts in the perpendicular direction $\theta_c + \pi/2$. The condition that z remains constant implies

$$G_1 + G_2 = z \tag{13}$$

and the anisotropy is given by

$$2(G_1 - G_2) = a\, z \tag{14}$$

This procedure can continue until either $G_1 = G_{\max}$ (*gain saturation*) or $G_2 = G_{\min}$ (*loss saturation*). By virtue of Equation13, when one of these two extremes is reached, the anisotropy can be increased no more with a fixed value of z. Hence, the largest anisotropy $a_{\max}(z)$ for a specified value of z is fixed either by Gain Saturation (GS) or by Loss Saturation (LS). Using Equations 13 and 14 we get

$$a_{\max}(z) = \min\left\{2\left(1 - \frac{z_{\min}}{z}\right), 2\left(\frac{z_{\max}}{z} - 1\right)\right\} \tag{15}$$

This function is shown in Figure 5. By construction, $a_{\max}(z_{\min}) = a_{\max}(z_{\max}) = 0$. The largest possible anisotropy a_{Max} is

$$a_{Max} = a_{\max}(z_{mean}) = 2\frac{z_{\max} - z_{\min}}{z_{\max} + z_{\min}} \tag{16}$$

for $z = z_{mean} = (z_{\max} + z_{\min})/2$. Using $z_{\min} = 3$ and $z_{\max} = 4$, we get $a_{Max} \approx 0.28$. According to Equation 15, $a_{\max}$ increases with z for $z < z_{mean}$, and it declines with z for $z > z_{mean}$. When the anisotropy $a = a_{Max}$ is reached along a monotonic path, the anisotropy and the coordination

can evolve no more since both contact gain and contact loss are saturated. This suggests that the steady state corresponds to the intersection between the two regimes, so that $\tilde{z} = z_{mean}$ and $\tilde{a} = a_{Max}$. Note that the expression of $a_{\max}(c)$ in Equation 12 has the same functional dependence on c as $a_{\max}(z)$ in Equation 15 on z in the gain saturation regime.

In Figure 6 we have shown an example of the evolution of the anisotropy a with the coordination number z in a biaxial compression test simulated by the contact dynamics method for two initially quasi-isotropic samples with different initial coordination numbers $z_0 = 3.1$ and $z_0 = 3.7$. The composition and the coefficient of friction ($\mu = 0.8$) are similar in the two samples. In both cases z tends to the same steady-state value $\tilde{z} \approx 3.35$ for which $\tilde{a} \approx 0.24$. From these values and using Equation 16 together with the assumption that $\tilde{a} = a_{mean} = (z_{\min} + z_{\max})/2$, we get $z_{\min} = 2.94$ and $z_{\max} = 3.75$. The saturation curve (Equation 15) is shown for these values in Figure 6. We see that in the gain saturation regime (as z decreases from $z_0 = 3.7$) the anisotropy reaches and then follows closely the saturation curve up to the steady state. Hence, in this regime, Equation 15 provides an excellent fit to the data with only one fitting parameter $z_{\max}$. In the loss saturation regime (as z increases from $z_0 = 3.1$), the data remain below the saturation curve, reached only at the steady state. Even with very slow shearing, the evolution of a loose sample from an initially isotropic state is strongly unstable and dynamic. As a result, the rearrangements at the initial stages of evolution (as long as the coordination number is low) do not give rise to an oriented gain of contacts. This leads to a slow increase of the anisotropy compared to the coordination number. This effect disappears as the coordination number becomes larger.

Coming back to the monotonic stress-strain behaviour, we see that the simple arguments developed above and partially corroborated by numerical simulations, allow us to characterize the steady state in a simple way and to distinguish two regimes: (a) $z_0 < \tilde{z}$ (initially loose system): since $z_0 < \tilde{z}$, z increases towards $\tilde{z}$ by gain of contacts. The system remains in the LS regime during its evolution towards the steady state. Hence, $a_{\max}$ and the shear strength, as a result, increase monotonically with z to saturate at their steady-state value; (b) $z_0 > \tilde{z}$ (initially dense system): since $z_0 > \tilde{z}$, z decreases towards $\tilde{z}$ by loss of contacts. The system remains in the GS regime. As a result, $a_{\max}$ and the shear strength increase until z reaches its steady-state value. It is also worth noting that shear localization need not worry us about the application of Equation 15 since the same mechanisms continue to be active *inside* the shear zones.[26,27]

6 EQUILIBRIUM STATES

The equilibrium states of a granular packing subjected to external forces are globally characterized by the probability distribution $p_e(\theta, N, T)$. This function contains (by integration) the distributions of contact directions ($p_\theta(\theta)$), normal forces ($p_N(N)$), friction forces ($p_T(T)$) and friction mobilization ($p_\eta(\eta)$, with $\eta \cong T/\mu N$), as well as force-fabric correlations. A major task in micromechanical modelling of granular plasticity is to deduce the

distribution $p_e(\theta,N,T)$ from *purely geometrical* descriptors of the microstructure such as g_c and p_c. This is a difficult task since numerical investigations reveal broad force distributions and ingenious force-fabric correlations. Often qualitative concepts such as "force chains" or "arching" are used to describe the patterns observed in experiments (optical visualization of stresses by means of the photoelastic effect, for example).[3] Here, we present a brief review of some outstanding properties of $p_e(\theta,N,T)$ with the motivation of understanding how a grain is equilibrated on average.

A peculiar aspect of force distribution, which we analyze in more detail here by focussing on normal forces, is the occurrence of numerous weak forces together with a number of strong forces appearing often sequentially (force chains).[3,6,28-30] The distribution p_N of normal forces in a macroscopically homogeneous system shows that about 57% of forces are below the mean force $\langle N\rangle$ and they have a *nearly* uniform distribution. They contribute only about 29% to the average pressure.[28] The number of forces larger than the mean decays almost exponentially.

The huge number of weak forces, as a consequence of grain frustrations or arching, with a nearly uniform distribution is a source of weakness for the system. Weak-force regions inside a packing correspond to locally weak pressures. Such regions are naturally more susceptible to fail. A quantitative analysis of grain rearrangements shows that during quasistatic evolution of the system, these weak regions undergo *local rearrangements*,[31] and nearly all sliding contacts (where the friction force is fully mobilized) are localized in weak regions.[7] Let $A(\xi)$ be the set of all contacts where the magnitude of the force is below a cutoff force ξ normalized by the mean force $\langle N\rangle$ in a macroscopically homogeneous packing. The set $A(\xi=\infty)$ corresponds then to the whole contact set. A simple analysis of simulation data shows that the fraction $\rho_s(\xi)$ of sliding contacts in the set $A(\xi)$ is not independent of ξ. Indeed, ρ_s increases with ξ from zero and tends to its largest value (8% for $\mu=0.5$) at $\xi\cong 1$, corresponding to the average force. This means that, sliding occurs almost exclusively at contacts carrying a force below the average force.

Another interesting property of weak contacts in a granular medium is that, in monotonic shearing, the weak contacts are on average perpendicular to the direction of strong contacts.[7] To show this, we consider the partial fabric tensor $\overline{\overline{F}}(\xi)$ defined as the restriction of the expression of $\overline{\overline{F}}$ (defined above) to the contacts belonging to the set $A(\xi)$. The corresponding anisotropy $a(\xi)$ is a function of ξ. A typical example of $a(\xi)$ is shown in Figure 7. In this figure, a positive value of a indicates that $\theta_c(\xi)$ (average contact direction in the set $A(\xi)$) is along the compression axis, i.e. $\theta_c(\xi)\approx\theta_\sigma$, whereas a negative value of a corresponds to the direction $\theta_\sigma+\pi/2$. We see that the direction $\theta_c(\xi)$ is *perpendicular* to the axis of compression ($a<0$) for weak forces ($\xi<1$). The anisotropy increases (in absolute value) as ξ increases, and reaches a maximum at $\xi=1$ corresponding to the average force. As ξ is further increased, a becomes less negative and finally changes sign at $\xi\approx 2$. This shows that the contacts which carry a force above the mean are preferentially oriented parallel to the axis of compression, and their positive contribution to a outweighs the negative contribution of the forces below the mean. Distinguishing in this way *strong contacts* (contacts where $N>\langle N\rangle$)

from *weak contacts* (contacts where $N < \langle N \rangle$), we decompose the fabric tensor and the anisotropy a as a sum of two terms with opposite phases:

$$a = a_s - a_w \tag{17}$$

where a_s and a_w are the (positive) anisotropies of the strong and weak contact sets, respectively. The weak fabric tensor $\overline{\overline{F}}_w$ is *orthoaxial* with the strong fabric tensor $\overline{\overline{F}}_s$.

A similar analysis can be applied to the stress tensor whose micromechanical expression is given by Equation 1. By restricting the averaging operation to the set $A(\xi)$, we get partial stress tensors $\overline{\overline{\sigma}}(\xi)$. In particular, let us consider the partial stress ratio $q(\xi)/p$ as a function of ξ; see Figure 8. Amazingly, for all $\xi < 1$, we have $q(\xi)/p \approx 0$! This means that nearly the whole *deviator* stress is carried by the strong contact set. The weak contact set contributes only to the average pressure. This suggests an additive decomposition of the stress tensor as following:[7]

$$\overline{\overline{\sigma}} = p_w \overline{\overline{I}} + \overline{\overline{\sigma}}_s \tag{18}$$

where $\overline{\overline{I}}$ is the unit tensor, p_w is the weak pressure (carried by the weak contact set) and $\overline{\overline{\sigma}}_s$ is the strong stress tensor (carried by the strong contact set). Numerical simulations show that $p_w/p \approx 0.29$. Hence, from the point of view of stress transmission, the weak contact set corresponds to a *liquidlike* phase whereas the strong contact set appears as the *solidlike* backbone of the medium transmitting deviatoric stresses. The same behaviour was observed also in three-dimensional granular media. Figure 9 shows the normal forces encoded as the width of segments joining particle centres, the two contact sets by two different grey levels, and the positions of sliding contacts, which belong almost exclusively to the weak set, in an assembly of 4000 grains subjected to biaxial compression by means of the contact dynamics method.

From the above analysis, we arrive at the following picture of the equilibrium of grains: strong forces act on the grains at contacts (inside the strong fabric) that are strongly *aligned* with the major principal direction of the stress tensor. Lateral weak forces (the weak fabric) prop the grains against *deviations* from alignment at strong contacts. In other words, the weak contacts play the same stabilizing role with respect to the grains supporting strong forces as the *counterforts* with respect to an architectural arch. Hence, this bimodal transmission of shear stresses may be understood as a ``tensorial arching effect'' that materializes the particular stress-fabric correlation that underlies the stability of a granular packing.

This particular stress-fabric correlation can be interpreted as a way of optimizing the capacity of the microstructure to support largest shear stresses. Indeed, according to Equation 4, the deviator stress q increases if a larger number of strong normal forces N occur at contacts aligned with the stress tensor ($\theta \approx \theta_\sigma$). This obviously leads to a surplus of weak contacts in the perpendicular direction. This mechanism can be compared to the loss-gain mechanism leading to the increase of structural anisotropy. In the loss saturation regime where no more contact loss is allowed along the direction of extension, either z evolves (together with $a_{\max}$) or the stress ratio increases as a result of *extra* weakening of contacts in the

direction of extension. Symmetrically, in the gain saturation regime where no more contact gain is allowed along the direction of compression, either z evolves (together with $a_{\max}$) or the stress ratio increases as a result of extra strengthening of contacts in the direction of compression. In both cases the force anisotropies a_n and a_t increase, leading to an increase of the stress ratio according to Equation 10.

7 FABRIC EVOLUTION

The incremental evolution of state variables with plastic strain determines the hardening properties of a granular material. Let $E[\theta-\theta_c(t)] \cong z(t)\, p_\theta[\theta-\theta_c(t)]$ be the distribution of contact directions at "time" t. The incremental evolution of the fabric is then given by the total derivative $\dot{E}(E,\dot{\overline{\overline{G}}})$ as a function of E and the velocity gradient tensor $\dot{\overline{\overline{G}}}$. Let θ_ε be the major principal direction of $\dot{\overline{\overline{G}}}$. The rotational invariance of the system implies that $\dot{E}$ is a function of $\theta_\varepsilon - \theta_c$. In other words, the fabric change at any moment depends on the direction θ_ε of loading with respect to the fabric.

Assuming that z and a follow the saturation curve $a_{\max}(z)$ (Equation 15), the evolution of the fabric is simply reduced to that of z: $\dot{z} = \dot{z}(z,\dot{\overline{\overline{G}}})$. Since z is an average over all directions, the deviator strain rate and rigid rotations are not expected to influence $\dot{z}$. Hence, only the volumetric strain rate $\dot{\varepsilon}_p$ should be taken into account, i.e. $\dot{z} = \dot{z}(z,\dot{\varepsilon}_p)$. The assumption of rate independence in quasistatic loading implies further that $\dot{z}$ depends on $\dot{\varepsilon}_p$ through a positively homogeneous function of degree 1. As a result,

$$\dot{z} = f(z)\,\dot{\varepsilon}_p \tag{19}$$

where $f(z)$ is an unknown function of z. Since the grains are assumed to be infinitely rigid, the volumetric strain rate $\dot{\varepsilon}_p$ represents only plastic volume increments (due to grain displacements). Figure 10 displays z as a function of the total volume change ε_p normalized by the initial volume in a numerical simulation with 4000 (circular) grains. The data is well fitted by the following form:

$$z = z_0 + (\tilde{z} - z_0)(1 - e^{-k\varepsilon_p}) \tag{20}$$

where $k \approx 1500$ is a numerical factor, and z_0 and $\tilde{z}$ are the initial and steady-state values of the coordination number, respectively. Such a large value of k indicates that tiny volume changes induce indeed large structural and stress changes in the system. We also observe that z reaches its steady-state value well before the solid fraction (ε_p continues to increase). Equation 20 implies $f(z) = k(\tilde{z} - z)$. Note also that, according to Equation 20, z increases if $z < \tilde{z}$, and it decreases in the opposite case. Equation 20 together with Equation 15 determines the evolution of the fabric along a monotonic path.

When the strain is reversed ($\theta_\varepsilon = \theta_c + \pi/2$ assuming $\theta_\varepsilon \approx \theta_c$ along a monotonic path) loss and gain directions, corresponding respectively to the directions of extension and compression, become orthogonal to the principal fabric directions. As a result, the fabric anisotropy, and the deviator stress, decreases and the principal fabric directions rotate similarly. The path in the (z,a) space is then below the saturation curve $a_{\max}(z)$. The fabric evolves until a new point on the saturation curve is reached. Along this path the fabric anisotropy a, its direction θ_c and the coordination number z are not subjected to gain or loss saturation constraints.

The evolution of E can be considered at the grain scale. Three elementary processes contribute to fabric change: contact *gain*, contact *loss* and contact *advection*. The latter refers to the rotation of *persisting* contact normals, corresponding thus to a *continuous* change in the contact direction, whereas the contact gain and loss are *discontinuous* (topological) changes in the fabric. Let $I^+(\theta)$ and $I^-(\theta)$ be respectively the gain and loss rates per grain along the direction θ. The contact *induction* function $I(\theta) = I^+(\theta) - I^-(\theta)$ represents the *net* change in the number of contacts due to gain and loss. Along a given direction, I is positive if there is more gain than loss, and it is negative if there is more loss than gain. We introduce also an *advection current* $J(\theta)$ corresponding to the mean current of persisting contacts at θ in the space of angles. Then, $\partial J/\partial\theta(\theta)$ is the mean change in the number of persisting contacts along θ due to contact rotations. The difference $I - \partial J/\partial\theta$ in each direction gives the variation $\partial E/\partial t$ of the number of contacts in that direction. Hence, E satisfies the following *balance equation*:[13,32]

$$\frac{\partial E}{\partial t} + \frac{\partial J}{\partial \theta} = I \tag{21}$$

The two functions I and J depend both on the fabric E and the velocity gradient tensor $\dot{\overline{\overline{G}}}$. The induction function I is naturally proportional to the relative normal velocity $v(\theta)$. In the same way, the advection function J is proportional to the relative tangential velocity $u(\theta)$ of grain centres. Since contact gain takes place between grains that are *not* in contact, we extend the contact network and the fabric, represented here by the function E, to such pairs of grains. In fact, simulations show that the fabric remains almost unchanged upon such an extension provided the "gap" is sufficiently small compared to the mean grain size. Then, $v(\theta)$ can take both positive values (when two grains approach to one another) and negative values (when two grains separate from one another) at potential contacts. By considering potential contacts, we simply assume a *prospective* point of view, i.e. we consider the *oncoming contacts* instead of outgoing ones.

As a result of steric exclusions the local velocities $v(\theta)$ and $u(\theta)$ are different from global (far-field) velocities which are dictated by the macroscopic velocity gradient tensor (in a homogeneously sheared assembly). Indeed, the application of an affine velocity field to a granular assembly leads to the interpenetration of touching grains. The local velocities thus provide a "correction" to the imposed velocity field, restoring the mutual exclusions of the grains. The local velocity field can be characterized by the probability density function $p_f(\theta,v,u)$ defined as the probability density for an effective or potential contact to have its direction along θ and where the relative normal and tangential velocities are v and u,

respectively. By definition, $p_\theta(\theta) = \int p_f \, dv\, du$. The distribution p_f allows the definition of average velocities $v_m(\theta)$ and $u_m(\theta)$ by

$$v_m(\theta)\, p_\theta(\theta) \equiv \int v\, p_f \, dv\, du \tag{22}$$

$$u_m(\theta)\, p_\theta(\theta) \equiv \int u\, p_f \, dv\, du \tag{23}$$

Figure 11 shows the mean steady-state velocity field (v_m, u_m) in the frame of a typical grain for different gaps in a simple shear simulation. We see that the near field (below a gap nearly equal to l_m) is considerably different from the far field. While the far field is a simple affine velocity field, the local field is inhomogeneous. The normal velocities are enhanced along the principal strain rate directions (at $\pm\pi/4$ to the vertical) and recirculation currents occur in front of the particle along the flow direction.

The detailed balance of contact events can be obtained by expressing I and J as a function of the local velocities $v_m(\theta)$ and $u_m(\theta)$. The advection current is the product of $u_m(\theta)$ and the density $\delta_J(\theta)$ defined as the mean number of contacts along the grain *circumference* ("surface" density in three dimensions) as a function of the contact direction θ. Considering an angular interval $\delta\theta$ at a distance l_m, this density is $\delta_J(\theta) = E(\theta)\,\delta\theta/(l_m\,\delta\theta) = E(\theta)/l_m$. The advection current is then given by

$$J(\theta) = \delta_J(\theta) u_m(\theta) = E(\theta) u_m(\theta)/l_m \tag{24}$$

The contact induction is the product of $v_m(\theta)$ and the *cross section* $\delta_I(\theta)$ given by the length element ("surface" element in three dimensions) $l_m\delta\theta$ times the mean number of contact neighbours per unit *area*, $E(\theta)\delta\theta/(1/2\,l_m{}^2\,\delta\theta)$, along the direction θ. Thus, the induction function is

$$I(\theta) = \delta_I(\theta)\, v_m(\theta) = 2E(\theta)\, v_m(\theta)/l_m \tag{25}$$

We need also to specify the local velocities $v_m(\theta)$ and $u_m(\theta)$ at effective or potential contacts as a function of the macroscopic velocity gradient tensor $\overline{\overline{G}}$. The simplest idea is to assume that the local velocity field is identical to the far field. Although this "affine assumption" contradicts the numerical observation displayed in Figure 13, it is still instructive to evaluate the outcomes of such an assumption for the fabric evolution. The mean local velocities at a distance l_m can be expressed as a function of the volumetric strain rate $\dot{\varepsilon}_p$, the deviator strain rate $\dot{\varepsilon}_q$ and the rigid rotation (semi-rotational of the velocity field) ω:

$$\frac{v_m(\theta)}{l_m} = \frac{\dot{\varepsilon}_p}{2} + \frac{\dot{\varepsilon}_q}{2}\cos 2(\theta - \theta_\varepsilon) \tag{26}$$

$$\frac{u_m(\theta)}{l_m} = \omega + \frac{\dot{\varepsilon}_q}{2}\sin 2(\theta - \theta_\varepsilon) \tag{27}$$

Now, we may look for a solution of the following form:

$$E(\theta,t) = \frac{z(t)}{2\pi}\left\{1 + a(t)\cos 2[\theta - \theta_c(t)]\right\} \tag{28}$$

Inserting the expressions of I, J, v_m, u_m and E in Equation 21, multiplying alternatively by 1, $\cos 2(\theta - \theta_c)$ and $\sin 2(\theta - \theta_c)$ and integrating each time with respect to θ, we get the following system of equations for fabric evolution:

$$\begin{cases} \dot{z} = z\,\dot{\varepsilon}_p \\ \dot{a} = \sqrt{2}\,\dot{\varepsilon}_q \cos 2(\theta_c - \theta_\varepsilon + \pi/8) \\ 2a(\dot{\theta}_c - \omega) = \sqrt{2}\,\dot{\varepsilon}_q \sin 2(\theta_c - \theta_\varepsilon - \pi/8) \end{cases} \tag{29}$$

The first equation is to be compared with Equation 19 for the monotonic case. The factor z is obviously well below $k(\tilde{z} - z)$ (with a large value of k) obtained for monotonic deformation. The second equation shows that the variation of the anisotropy depends on the direction θ_ε of loading with respect to the fabric direction θ_c. In particular, when $\theta_c - \theta_\varepsilon > \pi/4$, the anisotropy falls off ($\dot{a} < 0$). If $\omega \neq 0$, there is no steady-state solution. With a constant deviator $\dot{\varepsilon}_q$, the anisotropy grows and oscillates at the same time. However, in deriving Equation 29, we have assumed that a and z are independent parameters while in the steady state, or more generally along a monotonic path, they are linked together through the gain or loss saturation condition Equation 15. If $\omega = 0$, the steady-state solution ($\dot{a} = \dot{\theta}_c = 0$) is characterized by $\theta_c - \theta_\varepsilon = \pi/8$. Since θ_c tends to coincide with θ_σ (major principal direction of the stress tensor), this phase difference may be interpreted as *non-coaxiality* between stress and strain-rate tensors.

We get basically the same equations as Equation 29 if we use the *local* velocity gradient tensor. Then, $\dot{\varepsilon}_p$ and $\dot{\varepsilon}_q$ should be interpreted as the local spherical and deviator strain rates. The problem, however, is not in the distinction between the local and macroscopic strain rate tensors. The point is that the local velocities v_m and u_m involved in the balance equation are not related in a simple way as that assumed in Equations 26 and 27 (affine assumption) to the velocity gradient tensor. In fact, the local velocity field is inhomogeneous (see Figure 11) and it evolves with the fabric.

A simple way to circumvent this difficulty is to rely on Fourier expansions of $v_m(\theta)$ and $u_m(\theta)$ to the desired order. A similar approach was used for contact forces in Equations 8 and 9. The properties of the local velocity field are then reflected in the Fourier coefficients. To keep to the lowest nontrivial order (for E, v_m and u_m), let us set

$$\frac{v_m(\theta)}{l_m} = \frac{c_n \dot{\varepsilon}_p}{2} + \frac{b_n \dot{\varepsilon}_q}{2} \cos 2(\theta - \theta_\varepsilon) \tag{30}$$

$$\frac{u_m(\theta)}{l_m} = \omega + \frac{b_t \dot{\varepsilon}_q}{2} \sin 2(\theta - \theta_\varepsilon) \tag{31}$$

where the coefficients c_n, b_n and b_t may evolve with time or with the anisotropy. These expressions are more general than Equations 26 and 27, but preserve the same symmetries. Equations 30 and 31, together with Equations 21, 24, 25 and 28, yield the following system of equations for the evolution of the fabric parameters:

$$\begin{cases} \dot{z} = c_n z \dot{\varepsilon}_p \\ \dot{a} = b\, \dot{\varepsilon}_q \cos 2(\theta_c - \theta_\varepsilon + \lambda) \\ 2a(\dot{\theta}_c - \omega) = b \dot{\varepsilon}_q \sin 2(\theta_c - \theta_\varepsilon - \lambda) \end{cases} \tag{32}$$

with $b = \sqrt{b_n^{\,2} + b_t^{\,2}}$ and $\tan(2\lambda) = b_t / b_n$. The predictions are essentially the same as before, but there are now three parameters which can be adjusted. The parameter c_n allows for a more realistic estimation of the variations of z as a result of volume changes. The phase λ is zero only if $b_t = 0$, i.e. when the distortions of the contact network due to contact advection can be neglected compared to discontinuous changes resulting from loss and gain. This probably is the case in sufficiently dense and loose states and when $\omega = 0$. Then, the system tends to a state where the anisotropy increases linearly with deviator strain (until the saturation limit is reached) and $\theta_c = \theta_\varepsilon$. The case where $b_n = 0$ corresponds to the states where the coordination number does not evolve any longer, but the volume continues to change as a result of contact network distortions. Then, $\lambda = \pi/4$. If $\omega = 0$, the system tends to a state where the anisotropy increases linearly (if b remains constant) with deviator strain and $\theta_c = \theta_\varepsilon + \pi/4$. A less phenomenological description of fabric evolution requires a proper modelling of local velocities by accounting for steric constraints.

8 DILATANCY

When a granular material composed of rigid grains is deformed, irreversible changes in solid fraction ρ occur as a result of collective grain rearrangements. The solid fraction, as a geometrical property determined by the microstructure, may be considered as a descriptor of the microstructure and used as a *state* variable. When *free* volume changes are allowed, the solid fraction evolves with the applied deviatoric strain rate $\dot{\varepsilon}_q$. Reynolds' *dilatancy* refers to this incremental volume change produced by shearing and characterized generally by a dilation angle ψ: $\sin\psi \cong -\dot{\varepsilon}_p / \dot{\varepsilon}_q$ (The negative sign here ensures that negative values of the dilation angle correspond to contraction according to our sign conventions). The dilation angle ψ is thus a basic plastic flow property of a granular material, and like the internal angle of friction

φ, it has to be specified as a function of the fabric.[13] The assumption of rate independence in quasistatic loading implies that all rates, including $\dot{\varepsilon}_p$, should depend on $\dot{\varepsilon}_q$ through a positively homogeneous function of degree 1. As a result, ψ is independent of $\dot{\varepsilon}_q$.

While the internal angle of friction φ basically reflects the Coulomb friction law (at the contact scale), the dilation angle ψ is a purely *structural* property which has no counterpart at the contact scale. In fact, the Coulomb friction law can be seen as a non-associated rigid-plastic behaviour (no relative displacement normal to the slip plane).[13] Therefore, the normality rule is not expected to hold at the macroscopic scale. Experiments show, indeed, that ψ is generally different from φ.[10,11] If the fabric did not evolve with plastic strain (no state variable), then the volume would not change and we would have $\psi = 0$ as in the basic Coulomb model. Since the solid fraction is a function of the fabric, and fabric changes depend on the direction of loading, we expect that ψ is different for different principal strain rate directions. Formally, let us consider E as the lowest-order representation of the fabric. Then, the solid fraction $\rho(E)$ is a function of E. Deriving with respect to "time", we get $\dot{\rho} = -\rho\,\dot{\varepsilon}_q \sin\psi = \dot{\rho}[E, \dot{E}(E, \dot{\overline{\overline{G}}})]$. This shows that the dilation angle depends on $\theta_c - \theta_\varepsilon$, the coordination number z and the anisotropy a. The dependence on the loading direction has been observed in experiments.[10] For instance, it has been shown that the dilation angle for dense sand tested at $\theta_c - \theta_\varepsilon = \pi/2$ is comparable to that for loose samples at $\theta_c = \theta_\varepsilon$.[4]

Since the fabric evolution in Equation 32 is expressed in terms of strain rates, it is straightforward to get the following expression for the dilation angle:

$$\sin\psi = -\frac{\dot{z}}{z}\frac{b}{c_n \dot{a}}\cos 2(\theta_c - \theta_\varepsilon + \lambda) \tag{33}$$

As required, this expression depends on the loading direction and evolves with the coordination number and the anisotropy. Along a monotonic path, from Equation 15, we have

$$\dot{a} = \begin{cases} (2-a)\dfrac{\dot{z}}{z} & \text{loss saturation} \\ -(2+a)\dfrac{\dot{z}}{z} & \text{gain saturation} \end{cases} \tag{34}$$

Combining Equations 33 and 34, we get

$$\sin\psi = \begin{cases} \dfrac{-b}{c_n(2-a)}\cos 2(\theta_c - \theta_\varepsilon + \lambda) & \text{loss saturation} \\ \dfrac{b}{c_n(2+a)}\cos 2(\theta_c - \theta_\varepsilon + \lambda) & \text{gain saturation} \end{cases} \tag{35}$$

The largest value of ψ predicted by Equation 35 is fixed by the ratio b/c_n. Since c_n is large, ψ should be quite small unless we assume very large values of b. In fact, c_n (for z) and b (for a) should be of the same order of magnitude when discontinuous structural changes

dominate. This is the case in very dense and loose states. On the other hand, the steady state corresponds to $\psi = 0$ which implies $\theta_c = \theta_\varepsilon + \pi/4 - \lambda$.

The focus of this section was put on general trends and the relation between fabric evolution and dilatancy. The equations of fabric evolution together with the function $\rho(E)$ are sufficient for the estimation of dilatancy. The function $\rho(E)$ can be evaluated by a tessellation of space into void cells. For example, in the simple case of a regular packing with $z = 4$, it is easy to show that $\rho = \pi / 2\sqrt{4 - a^2}$, where a is the anisotropy of the cells. The statistics of valence numbers allows us to obtain an estimation of the mean value of ρ over the cells as a function of z, a and θ_c. However, both for fabric evolution (local velocities) and for the evaluation of ρ it seems necessary to introduce higher order microstructural information. But, one might still keep with z, a and θ_c as the most basic state variables provided phenomenological parameters are introduced.

9 CONCLUDING REMARKS

We discussed basic plastic properties of granular materials as they may be understood or modelled from the lowest order description of granular fabric. The average connectivity or compactness is characterized by the coordination number whereas the preferred orientations of contact normals are represented by the (lowest-order) fabric anisotropy and its direction. It was argued that in a material composed of rigid grains, the macroscopic behaviour is essentially rigid-plastic characterized by a single angle of internal friction as yield criterion. The heart of a microscopic approach is the dependence of this criterion and the solid fraction on the fabric, as *physical* state variables, and the evolution of the latter with plastic strain.

A model based on this approach is all the more successful as it meets the steric constraints and the requirement of grain equilibrium. This can be achieved by considering the local environments through the multicontact distribution functions that may contain the desired level of microstructural information. We introduced a particularly simple approach which is more global in nature but incorporates steric constraints and grain equilibrium through "limit states". The presence of these limit states, which without loosing generality can be isotropic or not, leads to "gain" and "loss" saturation regimes for the fabric. It was shown that the stress-strain behaviour along known stress paths matches this microscopic picture quite well provided the shear strength is an increasing function of the fabric anisotropy along a monotonic path. This point was studied in more detail by considering the micromechanical expression of the stress tensor, and it was shown that the shear strength depends linearly on the fabric anisotropy but also harmonically on the principal stress directions with respect to the fabric. Using numerical results, we also emphasized the generic "bimodal" nature of force transmission in a granular medium that suggests a mechanism (similar to loss and gain for contact anisotropy) that allows the system to optimize the force anisotropy and hence the shear strength.

The fabric and volume changes (along and below the saturation limits) were discussed in the light of a balance equation for gain, loss and advection of contact neighbours. A key point in the evaluation of gain, loss and advection rates is the local velocity field which was shown to be non-affine and inhomogeneous due to steric constraints. We studied the outcome of a simple non-affine assumption with three parameters which leads to equations for the evolution of the coordination number, the fabric anisotropy and its direction as a function of the deviator

strain and direction of loading. These equations predict an exponential evolution of the coordination number with volumetric strain, a linear evolution of the anisotropy with deviatoric strain and a generic non-coaxiality between the fabric and strain principal directions. Interpreted in terms of the dilation angle, they show that the dilation angle is harmonically dependent on the loading direction.

The granular plasticity is a vast domain mostly based on phenomenological interpretation of experimental tests. Before a microscopic approach can reach the same predictive level, the main objective is to *understand* the trends from the lowest-level description of the microstructure. This was the main goal of this contribution, but not the only one. It is also important to note that even basic understanding of shear strength and fabric evolution properties requires further investigation of the fabric behaviour, local velocities and space correlations along *complex* loading paths. This is a major challenge due to demanding statistics both for experiments, which provide only limited information about the fabric, and for numerical discrete element methods, which do not allow for a large number of grains to be simulated at the same time. In this context, a model based on a hierarchical description of the fabric can provide a useful strategy allowing us to design genuine simulations or experiments in order to establish the relevant parameters and the level of description to be used in a particular application.

References

1. P. G. de Gennes, *Rev. Mod. Phys*., 1999, **71**, S374.

2. H. M. Jaeger and S. R. Nagel, *Rev. Mod. Phys.*, 1996, **68**, 1259.

3. P. Dantu, Proceedings of the 4th International Conference on Soil Mechanics and Foundation Engineering, Butterworths Scientific Publications, London, 1957, **1**, 144.

4. M. Oda, *Soils and Foundations*, 1972a, **12**, 17; 1972b, **12**, 1.

5. P. A. Cundall and O. D. L. Stack, *Geotechnique*, 1979, **29**, 47.

6. P. A. Cundall, A. Drescher and O. D. L. Strack, IUTAM Conference on Deformation and Failure of Granular Materials, Delft, 1982, 355.

7. F. Radjai, D. E. Wolf, M. Jean and J. J. Moreau, *Phys. Rev. Lett.*, 1998, **80**, 61.

8. M. R. Kuhn, *Mechanics of Materials*, 1999, **31**, 407.

9. F. Radjai and S. Roux, *Phys. Rev. Lett.*, 2002, **89**, 064302.

10. J. K. Mitchell, *Fundamentals of Soil Behaviour*, Wiley, New York, 1993.

11. D. M. Wood, *Soil Behaviour and Critical State Soil Mechanics*, Cambridge University Press, Cambridge, 1990.

12. M. Satake in Proceedings of the IUTAM Symposium on Deformation and Failure of Granular Materials, Delft, ed. P. A. Vermeer and H. J. Luger, Balkema, Amsterdam, 1982, 63.

13 S. Roux and F. Radjai in "Mechanics for a New Millennium", ed. H. Aref H. and J. Philips, Kluwer, Netherlands, 2001, 181.

14. H. Troadec, F. Radjai, S. Roux and J. C. Charmet, *Phys. Rev. E*, 2002, **66**, 041305.

15. J. J. Moreau J. J. in "Nonsmooth mechanics and applications", CISM Courses and Lectures, 1988, **302**, 1.

16. J. J. Moreau J. J., *Eur. J. Mech. A*, 1994, **13**, 93.

17. M. Jean and J. J. Moreau, Proceedings of Contact Mechanics International Symposium, Presses Polytechniques et Universitaires Romandes, Lausanne, Switzerland, 1992, 31.

18. J. Christoffersen, M. M. Mehrabadi and S. Nemat-Nasser, *J. Appl. Mech.*, 1981, **48**, 339.

19. L. Rothenburg and R. J. Bathurst R. J., *Geotechnique*, 1989, **39**, 601; R. J. Bathurst and L. Rothenburg, *Mechanics of Materials*, 1990, **9**, 65.

20. B. Cambou, in "Powders and Grains 93", ed. C. Thornton, Balkema, Amsterdam, 1993, 73.

21. A. Schofield and P. Wroth, *Critical State Soil Mechanics*, McGraw-Hill, London, 1967.

22. S. Roux and F. Radjai F in "Physics of Dry Granular Media", ed. Herrmann H. *et al*., Kluwer, Dordrecht, 1999, 229.

23. J. P. Troadec and J. A. Dodds in "Disorder and Granular Media", ed. D. Bideau and A. Hansen, Elsevier, Amsterdam, 1993.

24. F. Calvetti, G. Combe and J. Lanier, *Mech. Coh. Frict. Materials*, 1997, **2**, 121.

25. S. Torquato, *Random Heterogeneous Materials*, Springer, Berlin, 2001.

26. J. P. Bardet and J. Proubet, *Geotechnique*, 1991, **41**, 599.

27. J. Desrues, R. Chambon, M. Mokni and F. Mazerolle, *Geotechnique*, 1996, **46**, 529.

28. F. Radjai, M. Jean, J. J. Moreau and S. Roux, *Phys. Rev. Lett.*, 1996, **77**, 274.

29. D. M. Mueth, H. M. Jaeger and S. R. Nagel, *Phys. Rev. E*, 1998, **57**, 3164.

30. S. J. Antony, *Phys. Rev. E*, 2001, **63**, 011302.

31. L. Staron, J.-P. Vilotte and F. Radjai, *Phys. Rev. Lett.*, 2002, **89**, 204302.

32. F. Radjai and S. Roux in "Powders and Grains 2001", ed. Y. Kishino, Balkema, Tokyo, 2001, 21.

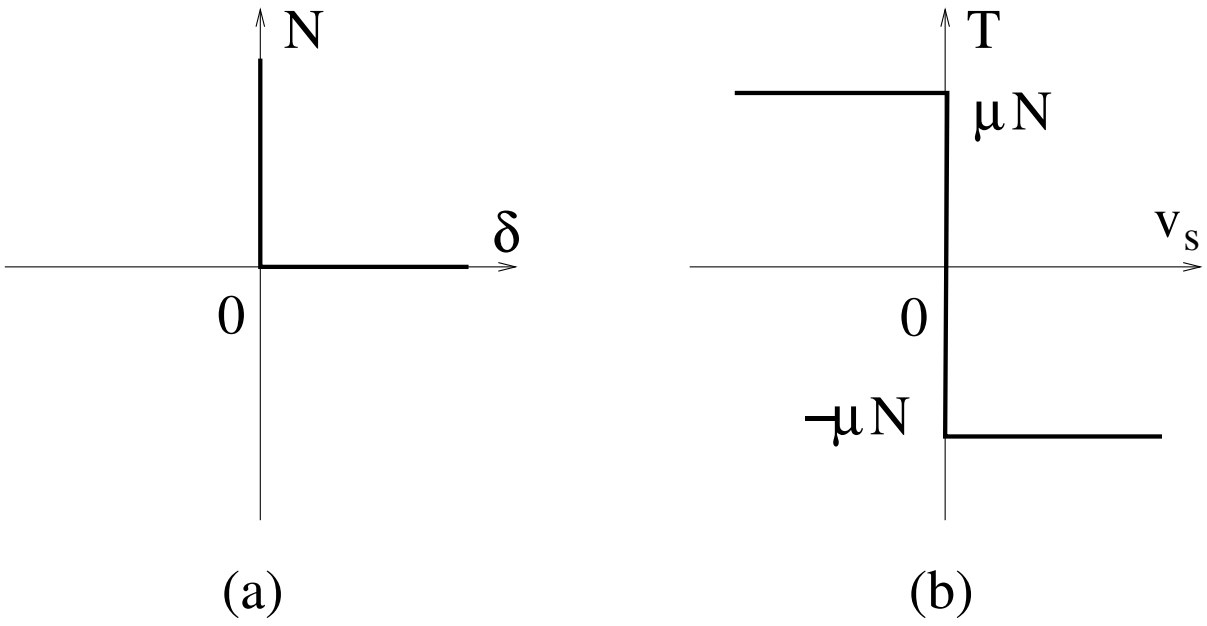

Fig. 1: *Nonsmooth contact laws: (a) Signorini condition, (b) Coulomb friction law*

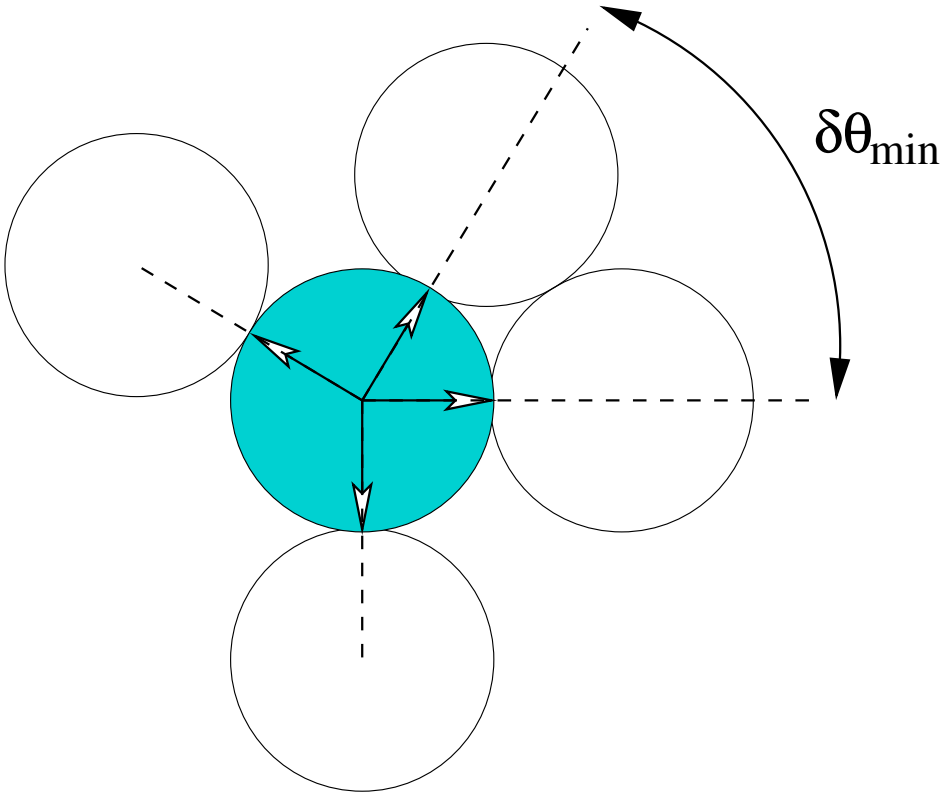

Fig. 2 *Illustration of angular exclusions*

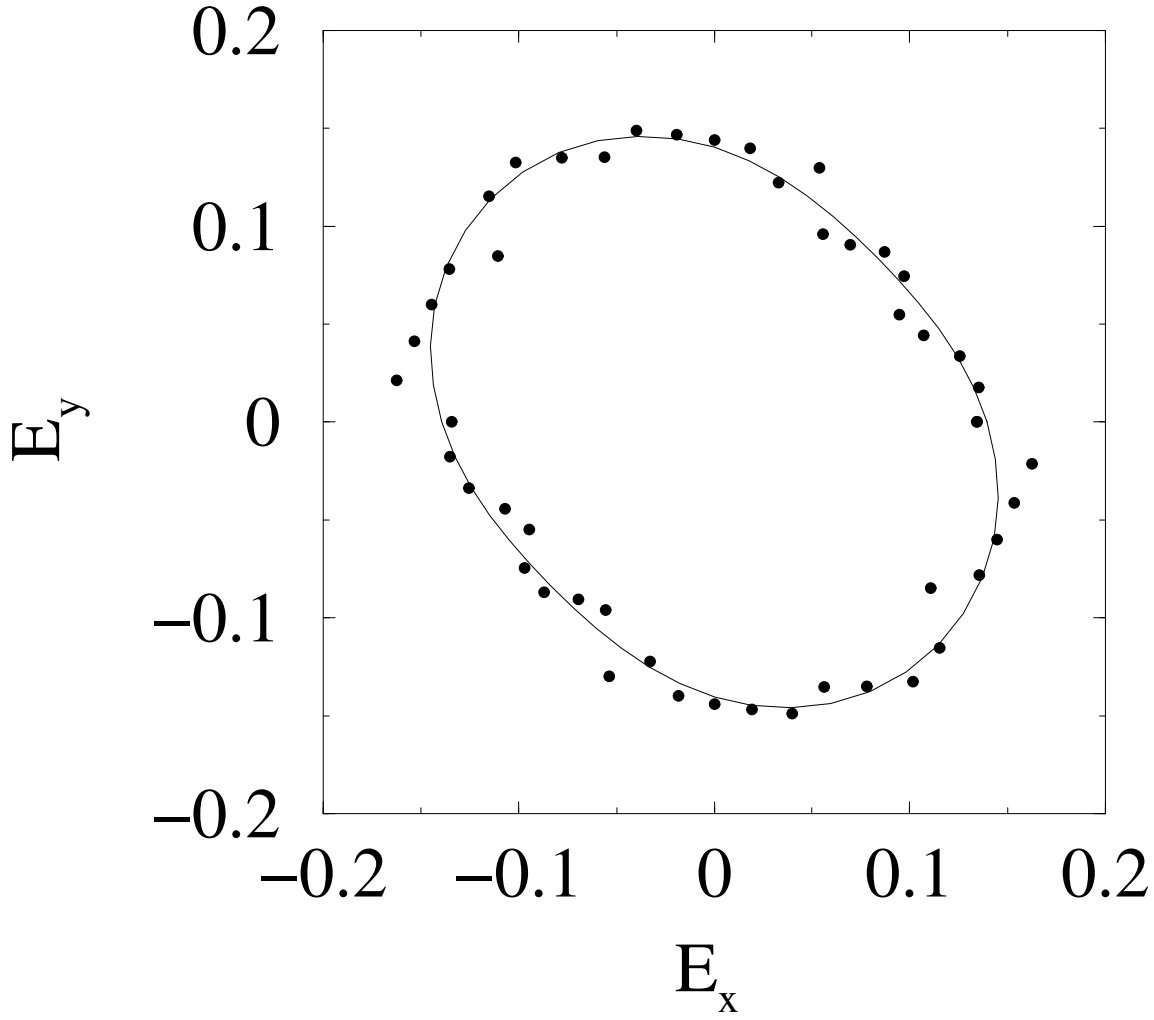

Fig. 3: *Polar representation of the distribution function of contact normal orientations in a simple shear simulation. The function is normalized such that its integral is equal to the coordination number (see the definition of function* $E(\theta)$ *defined in the text).*

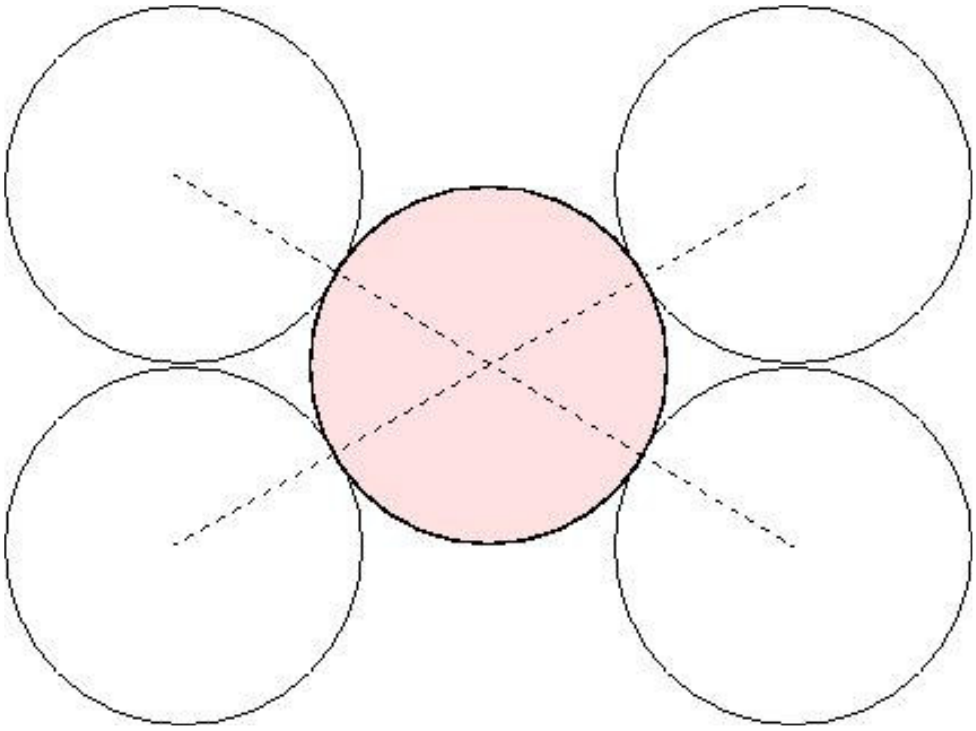

Fig. 4: *A local configuration with four contact neighbours presenting the largest local anisotropy.*

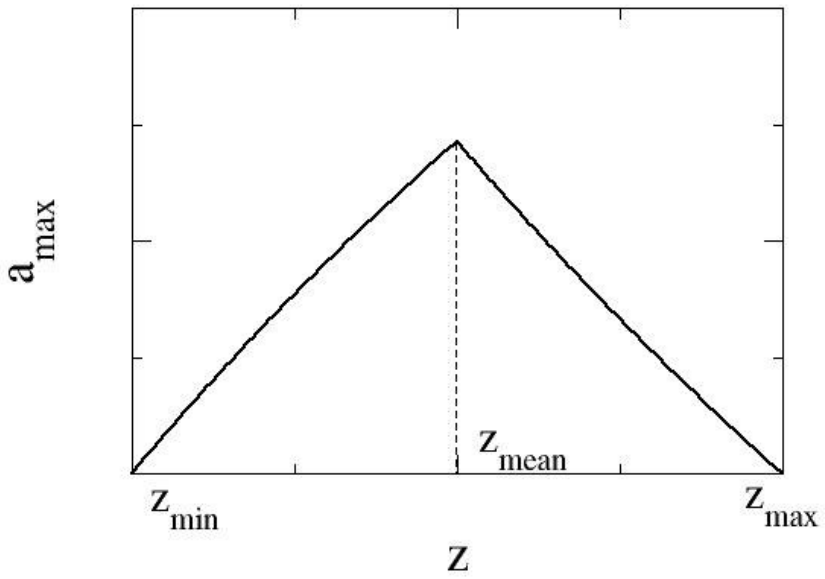

Fig. 5: *Maximal anisotropy* $a_{\max}$ *as a function of coordination number* z .

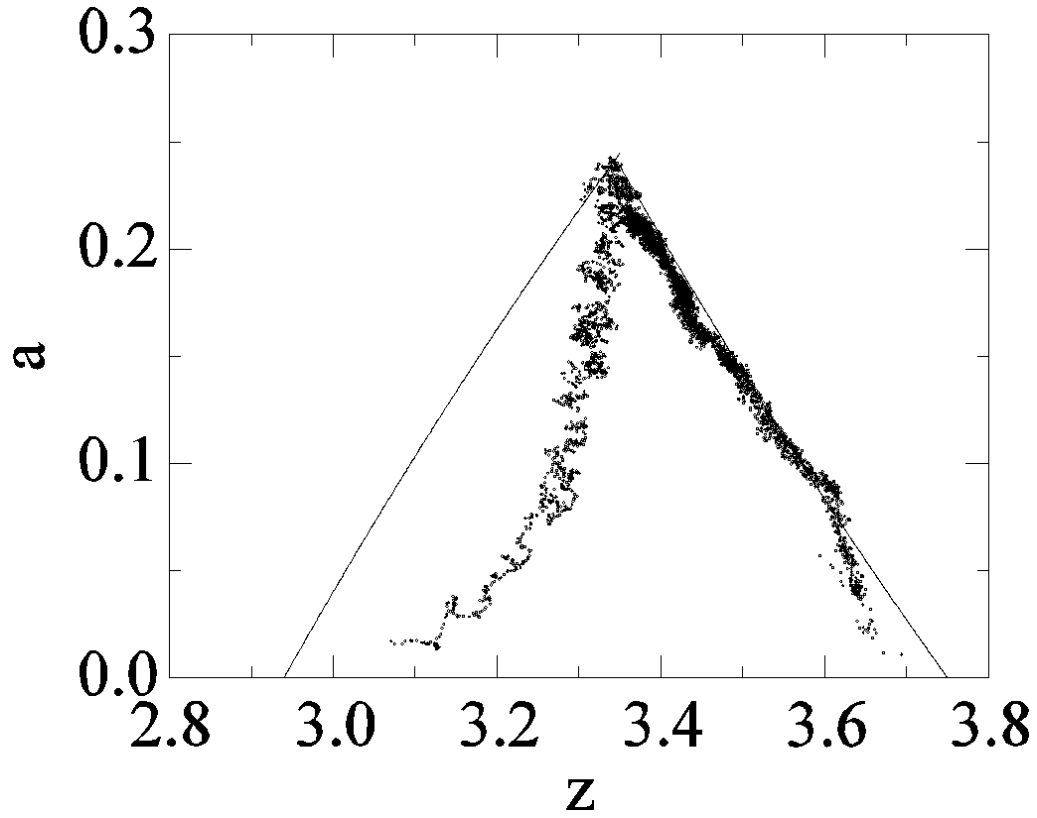

Fig.6: *Evolution of the anisotropy a with the coordination number z in a biaxially compressed assembly of rigid grains simulated by the contact dynamics method for an initially dense (right curve) and an initially loose (left curve) sample. The plain curve corresponds to the theoretical prediction (Equation 15).*

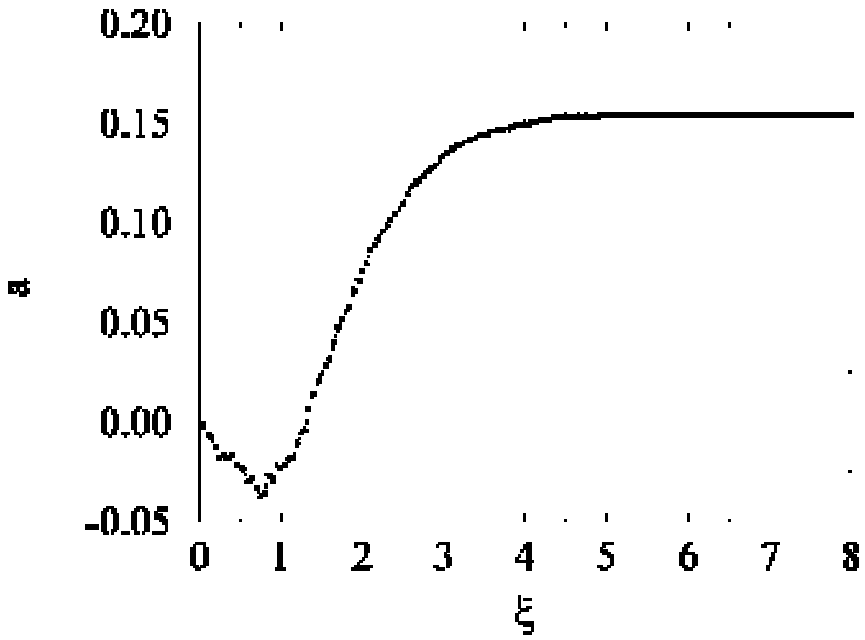

Fig. 7: *Partial anisotropy a as a function of the cutoff force ξ in a sheared grain assembly.*

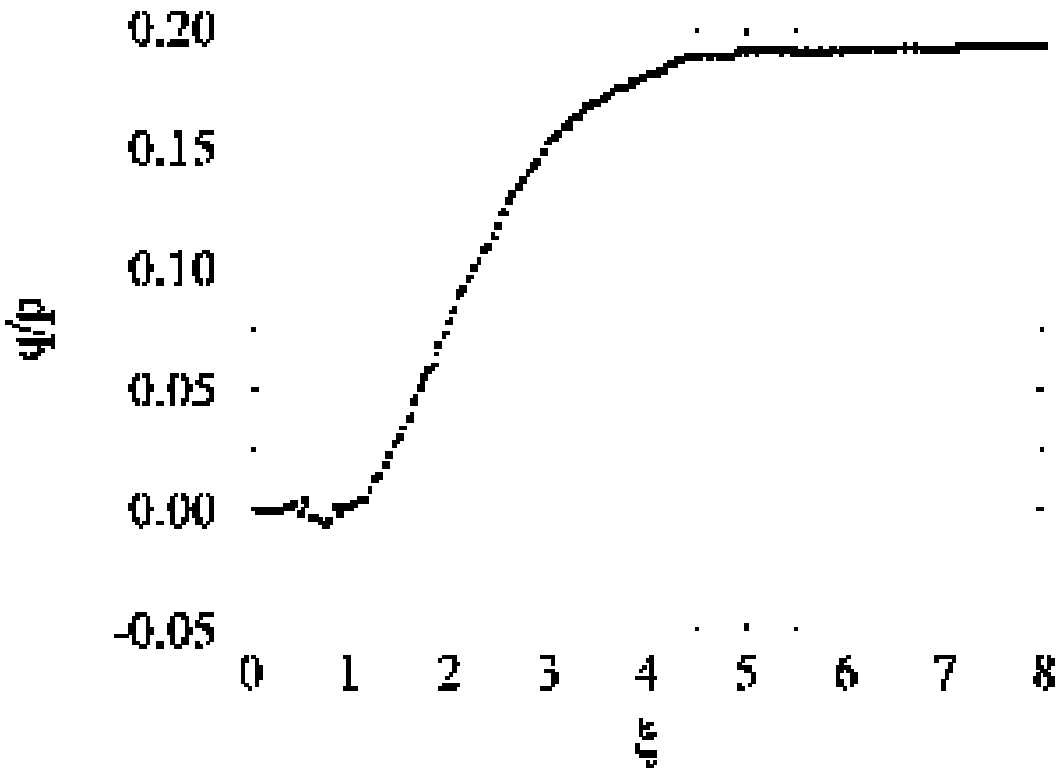

Fig. 8 : *Partial stress ratio* q/p *as a function of* ξ *in a sheared grain assembly.*

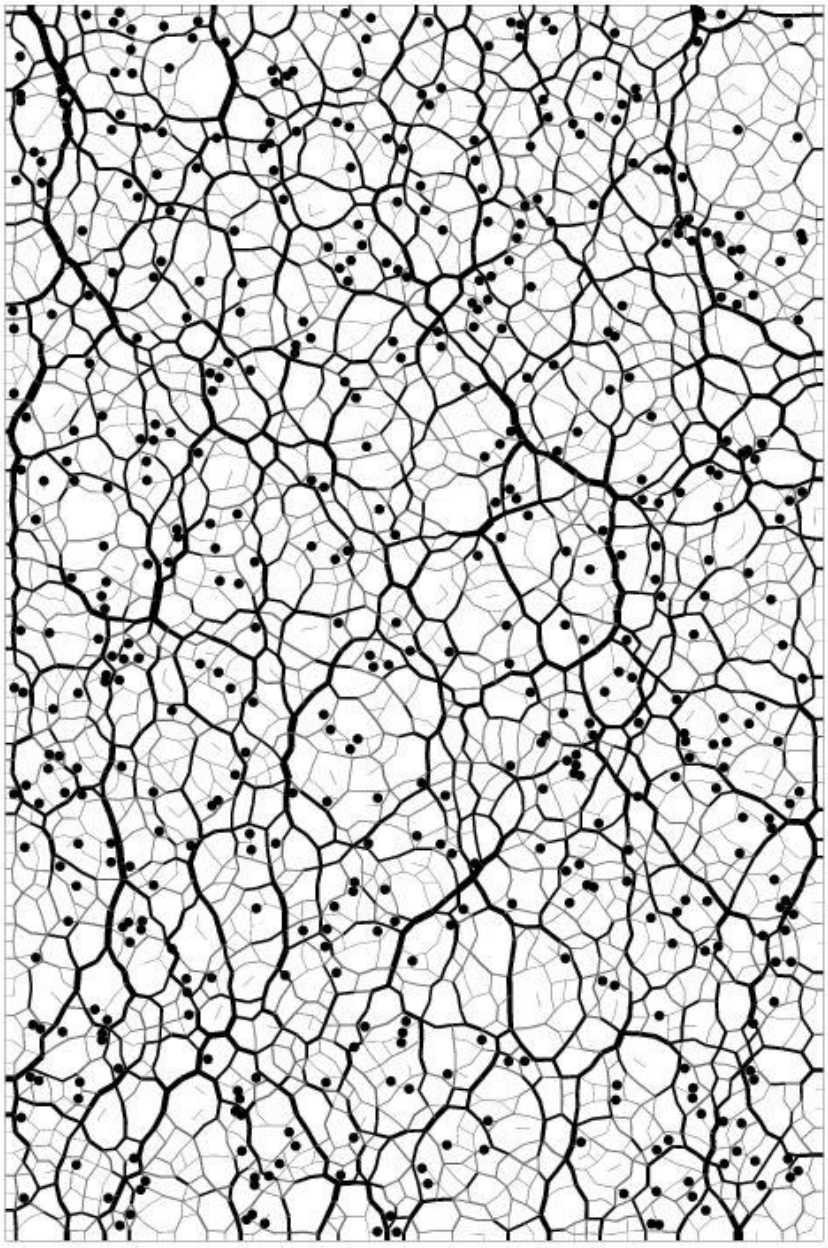

Fig. 9: *A map of normal forces in a biaxially sheared granular assembly. The width of segments joining particle centres are proportional to the normal force. The strong and weak contacts are shown in black and grey, respectively. Full circles show the positions of sliding contacts.*

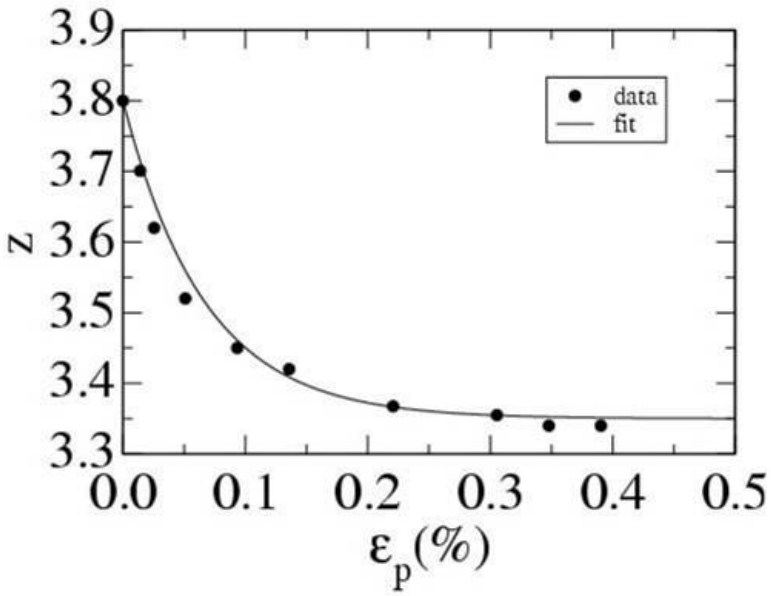

Fig. 10 : *Evolution of the coordination number* z *as a function of the volumetric strain* ε_p

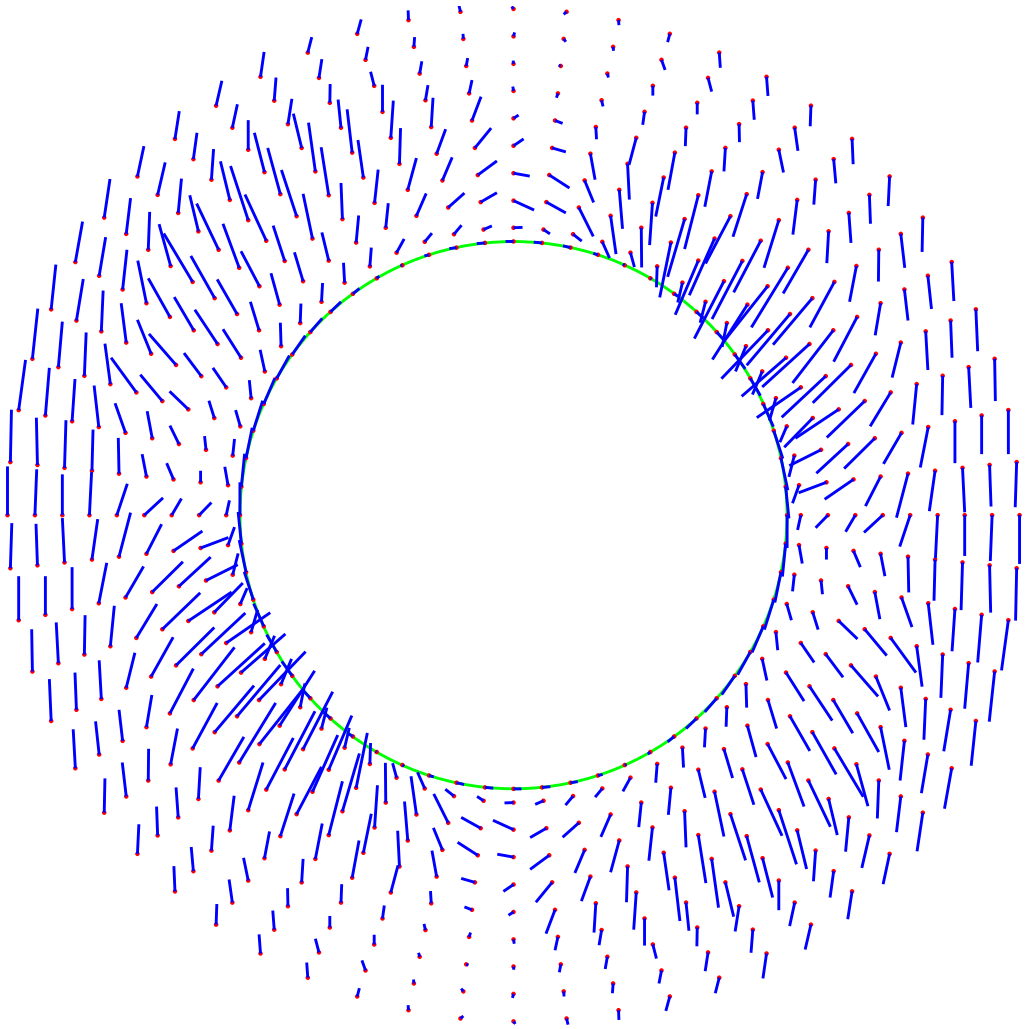

Fig. 11 : *The mean velocity field in the vicinity of a typical grain in a steady shear flow.*